A STUDY OF TURBULENT WAKES IN CONSTANT STREAMWISE PRESSURE GRADIENTS

Terrance Edwards Anderson

NAVAL POSTGRADUATE SCHOOL
Monterey, California

THESIS

A STUDY OF TURBULENT WAKES
IN
CONSTANT STREAMWISE PRESSURE GRADIENTS

by

Terrance Edwards Anderson

Thesis Advisor: G.J. Hokenson

March 1973

A Study of Turbulent Wakes
in
Constant Streamwise Pressure Gradients

by

Terrance Edwards Anderson
Lieutenant, United States Navy
B.I.E., Georgia Institute of Technology, 1965

Submitted in partial fulfillment of the
requirements for the degree of

MASTER OF SCIENCE IN AERONAUTICAL ENGINEERING

from the

NAVAL POSTGRADUATE SCHOOL
March 1973

ABSTRACT

Two-dimensional turbulent wakes in constant adverse and favorable pressure gradients were studied experimentally. The static and dynamic pressures through the wake were obtained with calibrated Prandtl-type pitot-static probes, and a computer program was written to extract from these data the velocity profiles, displacement thickness, momentum thickness, and the shape factor. This program further provides the turbulent shear coefficient, eddy viscosity, and Prandtl mixing length within the wake.

A wind tunnel was designed specifically for this experiment and its construction details are included. The tunnel test section is unique in that it can be adjusted to generate any specified adverse or favorable pressure gradient.

The results of the experiment indicated that the eddy viscosity was a function of the history of the flow rather than of the local mean flow field, as is classically assumed. The reaction of the turbulent wake to a favorable pressure gradient after encountering an adverse pressure gradient was significantly different from the reaction of the wake to only a favorable pressure gradient.

TABLE OF CONTENTS

LIST OF FIGURES

NOMENCLATURE

A = cross-sectional area

$| \; |$ = indicates absolute value

A_τ = turbulent exchange coefficient (Eq. 3, Introduction)

α = constant in Prandtl's eddy viscosity (Eq. 5, Introduction)

b = width of mixing region (Eq. 5, Introduction)

β = constant in test section area distribution (Eq. 7, Appendix A)

C_1 = volumetric flow rate through the test section

C_2 = negative of the test section pressure gradient (Appendix A)

C_τ = turbulent shear coefficient = $\tau / \frac{1}{2}\rho u^2 e$

d = wake generator diameter

$\frac{d}{dx}$ = indicates differentiation with respect to x

$\frac{\partial}{\partial x}$ = indicates partial differentiation with respect to x

δ^* = displacement thickness

ε = eddy viscosity = $\tau / \frac{\partial \bar{u}}{\partial y}$

exp = indicates exponentiation

F = arbitrary example function

H = shape factor = δ^*/θ

i = indicates i direction (i = 1,2,3)

∞ = large distance in the cross-streamwise direction

j = indicates j direction (j = 1,2,3)

L = length of pressure gradient

ℓ = Prandtl's mixing length (Eq. 4, Introduction)

ln = logarithm to base e

μ = laminar coefficient of viscosity

o = wake centerline conditions

p = static pressure

q = dynamic pressure = $\frac{1}{2}\rho V^2$

ρ = fluid density

σ_{ij} = stress tensor in Navier-Stokes equations

$\bar{\sigma}_{ij}$ = mean flow stress tensor in the time averaged Navier-Stokes equations

t = indicates time

T = indicates the characteristic period used for time averaging

τ_{ij} = Reynolds shear stress tensor

θ = momentum thickness

$\bar{u}$ = mean velocity in the x-direction

u' = fluctuating velocity in the x-direction

$\bar{u}_i, \bar{u}_j$ = mean velocity in i,j directions (i,j = 1,2,3)

u_i', u_j' = fluctuating velocity in i,j directions (i,j = 1,2,3)

$\bar{v}$ = mean velocity in the y-direction

v' = fluctuating velocity in the y-direction

V = one dimensional mean flow velocity

x = streamwise coordinate

x = j coordinate

y = cross-streamwise coordinate

y = lateral position at which C_τ is being calculated (Eq. 5, Appendix B)

Subscripts

e = local external flow conditions

i,j = directionality parameter ($i,j = 1,2,3$)

max = maximum value within the wake

min = minimum value within the wake

τ = shear related quantity

x,y = indicates partial differentiation with respect to x and y

1 = test section inlet conditions

2 = test section exit conditions

Superscripts

$\overline{}$ = indicates a time averaged quantity

$'$ = designates a fluctuating quantity

I. INTRODUCTION

When tangential stresses are applied to a fluid having internal friction, shearing motions are set up in line with the stresses and in conformity to the shape of the boundaries. Within this flow field, various kinds of secondary motions become possible. Regular ones, when they occur, are readily accounted for in terms of pressure gradients resulting from the curvature of the main flow, usually imposed by the shape of the boundaries. Irregular ones, called turbulence, are by far the more common, and their direct cause is less obvious. Their occurrence does not depend on the shpae of the boundaries, but like all secondary flows they must depend on a generating mechanism within the flow itself. According to present evidence the initial onset of turbulence occurs suddenly by a breakdown of the laminar flow in localized regions. Turbulence is convected downstream in the manner of any other fluid property and washed away from its point of origin. Repeated breakdowns are therefore generally required to maintain a continuous supply of turbulence, and instability of laminar flow is an essential part of this process.

In treating turbulence mathematically it is generally assumed that the motion can be separated into a mean flow, whose components are $\overline{u}_i$ (Cartesian tensor notation), and a superimposed fluctuating motion whose components are u_i', the

mean values of which are zero. For the flow of an incompressible Newtonian fluid, this decomposition can be applied to the dependent variables of the Navier-Stokes equations and time-averaged, the latter defined as

$$\overline{F}(x,y) \equiv \frac{1}{T} \int_{t}^{t+T} F(x,y,t)dt \qquad (1)$$

where T is a period of time large compared with the characteristic time of the turbulent oscillations. The resulting time-smoothed Navier-Stokes equations are

$$\rho \frac{\partial \overline{u}_i}{\partial t} = \frac{\partial}{\partial x_j} (\overline{\sigma}_{ij} - \rho \overline{u}_i \overline{u}_j - \rho \overline{u_i' u_j'}) \qquad (2)$$

These equations have the same form as the original Navier-Stokes equations if σ_{ij} is replaced by $\overline{\sigma}_{ij} - \rho \overline{u_i' u_j'}$. Thus the equations for the mean flow are the same as the original equations of motion, except that there are additional virtual stresses, $\tau_{ij} = -\rho \overline{u_i' u_j'}$, which represent the mean rate of transfer of momentum across a surface due to the velocity fluctuations. These virtual stresses were first introduced by Osborne Reynolds and are known by his name [Ref. 4].

The quantities u_i' and u_j' are the velocity fluctuations in the i- and j- directions at one point in space and $\overline{u_i' u_j'}$ is a measure of the correlation between the fluctuations. Correlations between fluctuations at two points in space are also measurable and give the size and orientation of

the turbulent eddies. In trying to solve analytically for the second-order correlation tensor, the solution is given in terms of third-order correlations. Similarly, the solution for the third-order correlation is given in terms of the fourth-order correlation, and so on. Hence the system cannot be closed and it is impossible to solve exactly for the second-order correlations [Ref. 1].

The various methods for the calculation of the turbulent flow field developed to date are based on empirical hypotheses. These approaches endeavor to establish a relationship between the Reynolds stresses produced by the fluctuating velocities and the mean values of the velocity components and their spatial derivatives. By this means, the virtual stresses are given an analytical form which closes the system of equations and constitutes the starting point for the calculation of the mean flow.

The first hypothesis relating the Reynolds stress to mean flow properties was advanced by Boussinesq and introduced a turbulent mixing coefficient, A_τ, such that the turbulent shear stress could be written

$$\tau = A_\tau \frac{d\bar{u}}{dy} \tag{3}$$

This coefficient corresponds to the viscosity, μ, in laminar flow and is therefore often called the "virtual" viscosity. Equation (3) has the great disadvantage that the virtual

viscosity, A_τ, is not a property of the fluid, as μ is, but depends on the structure of the flow field.

In 1925 Prandtl proposed his mixing length hypothesis in which the turbulent stresses are modelled as follows:

$$\tau = \rho \ell^2 \left|\frac{d\bar{u}}{dy}\right| \frac{d\bar{u}}{dy} \qquad (4)$$

The mixing length, ℓ, is that distance in the transverse direction which must be covered by an aggregation of fluid particles, travelling with its original mean velocity, in order to make the difference between its velocity and the velocity in the new lamina equal to the mean transverse fluctuations in the turbulent flow. The mixing length is still not a property of the fluid, but it is, in theory, a purely local function and it is far simpler to make plausible assumptions concerning the mixing length, ℓ, than for the virtual viscosity, A_τ. This constitutes the essential superiority of Prandtl's equation over that due to Boussinesq. Even so, Equation (4) is unsatisfactory in that the apparent kinematic viscosity, $\varepsilon = \ell^2 \left|\frac{d\bar{u}}{dy}\right|$ vanishes at points where $\left|\frac{d\bar{u}}{dy}\right|$ is equal to zero, that is at points of maximum and minimum velocity, which is contradictory to experimental evidence. A simpler expression for ε, also proposed by Prandtl which overcomes this problem is

$$\varepsilon = \alpha b (\bar{u}_{max} - \bar{u}_{min}) \qquad (5)$$

and is valid only for free turbulence, where α is an experimentally determined, dimensionless constant and b is the width of the mixing zone. Thus ε, for all the classical models of Reynolds stresses, remains constant over the whole width of the wake and is a function of the local mean flow.

Several other similar hypotheses have been proposed as analytical expressions for the Reynolds stresses which will only be mentioned here. They include: Taylor's vorticity transport theory, Von Karman's similarity hypothesis, and the universal velocity distribution law, each of which is linked to the mixing length concept due to Prandtl. Each of the aforementioned theories is valid only for free turbulent flow. While none of the theories adequately models the turbulent process in general, they are useful tools in the integration of the equations of motion in special cases.

In this investigation it was desired to ascertain, at least qualitatively, whether the virtual viscosity could be considered to be a function of the local mean flow properties in the case of two-dimensional turbulent wakes in constant favorable and adverse pressure gradients. A wind tunnel was designed and fabricated for this study which incorporated a variable-geometry test section that could be set to provide any specified pressure gradient. While this study was carried out using pitot-static probes as data sensors, it is anticipated that the flexibility and utility of the wind tunnel test section will allow a very detailed analysis of the turbulent wake using a hot-wire anemometer. This will also

permit the assessment of more modern eddy viscosity models which involve hypotheses with regard to the dependence of the shear on the turbulent kinetic energy.

II. THE WIND TUNNEL

A. INLET

The inlet bellmouth shown in Fig. 1 was constructed from eight-inch diameter aluminum pipe halves formed into a two-feet square inlet section. The corner seams, which were exposed to the inlet air flow, were filled with epoxy putty, hand formed, and sanded into a smooth fillet. This was done to smoothly transition the flow around these corners into parallel flow.

Immediately downstream of the inlet bellmouth was the plenum section of the tunnel. It consisted of four two-feet square by one foot long steel sections bolted together. Cork gaskets were inserted between the sections to prevent the influx of air at the joints and allow for smooth air flow over these junctions. Finally, two copper screens of #16 mesh between the first two and last two sections reduc d the ambient turbulence level in the flow prior to its entering the nozzle.

Initial operation of the tunnel indicated the presence of swirling in the air flow through the test section. This swirling was eliminated by the insertion of a four-inch thick, two-feet square section of quarter-inch honeycomb just prior to the first copper screen.

B. NOZZLES

Two different nozzles were constructed and used during the course of this investigation. One nozzle, used with the favorable pressure gradient test section, was constructed from half-inch Plexiglas. The nozzle, shown in Fig. 2, is two feet long, has an exit area of 168 square inches, (24 inches high by 7 inches wide), and a contraction ratio of 3.42. The top and bottom sides of the nozzle are parallel while the vertical sides contract to form the nozzle. The wake generator was attached to the nozzle in its exit plane on the axial centerline of the vertical walls. Static pressure ports were located at the nozzle entrance and exit planes along the axial centerline of the bottom wall. These were used to determine the nozzle exit (test section entrance) dynamic pressure, which determines the magnitude of the test section pressure gradient (see Appendix A).

The second nozzle was made from steel and was used with an adverse pressure gradient test section configuration. This nozzle, shown in Fig. 1, is two feet long, has an exit area of forty nine square inches (seven inches square) and a contraction ratio of 11.76. Static pressure ports were located on the right side of the nozzle at the inlet and exit for the purpose of determining the exit dynamic pressure. The wake generator was not mounted in the nozzle because of the difficulty encountered in trying to center and align it in the metal; rather in this case it was mounted just at the entrance of the test section.

C. WAKE GENERATORS

The wake generators were smooth Plexiglas cylinders spanning the width of the tunnel. A one inch diameter cylinder was used with the steel nozzle and a two inch diameter cylinder was used with the Plexiglas nozzle; thus "equivalent" turbulent wakes (see Results) were generated for each test section configuration. The wake velocity defect and turbulence resulted from flow separation of the turbulent boundary layers on the cylinders.

D. TEST SECTION

As shown in Fig. 3, the test section consisted of two parallel, vertical side walls separated by flexible and adjustable top and bottom walls, all made of Plexiglas. The flexible walls were made from one-eighth inch Plexiglas and fastened to the nozzle with piano hinges. Eight adjustment points, each with two threaded rods, allowed these walls to be positioned to any desired area distribution and horizontally levelled so that the test section geometry would remain rectangular throughout. Appendix A contains the development of the relationship between the pressure gradient and area distribution, based on a one-dimensional analysis. Table I contains the dimensions necessary to set the area profiles and form the two pressure distributions used in this study.

The right hand vertical wall of the test section contained thirteen slots through which the pitot-static probes were

inserted into the flow. These slots were nineteen inches high, three-eighths inch wide and spaced five inches apart. A teflon sliding seal prevented the influx of air through the slot in which the probe was being traversed. A filler plug for each unused slot was carefully hand milled and polished to make it conform perfectly with the flow side of the wall, thus eliminating the possibility of the plugs protruding into the flow and inducing separation. A thin aluminum strip wedged over each filler plug insured a tight fit.

The left hand vertical wall of the test section contained three rectangular access holes equally spaced along the axial centerline. These enabled the operator to remove and insert the wake generators, measure the probe position accurately, and level the lower adjustable wall. Also, along the axial centerline of this wall were thirty-three static pressure ports spaced one-and-a-half inches apart. A manometer bank connected to these ports gave a visual indi cation of the linearity and uniformity of the pressure distribution. The manometer also served to indicate any regions of separation, as did several rows of tufts which were attached to the walls of the adverse pressure gradient test section.

E. DIFFUSER AND MOTOR

The test section was followed by two seven-inch square, four feet long steel sections, a diffuser section and a

centrifugal blower driven by an electric motor shown in Figure 4. The diffuser was attached to the blower by a rubber buffer section which reduced the amount of bivration transmitted from the motor to the tunnel. The centrifugal blower, operated at three thousand revolutions per minute, pulled air through the tunnel and exhausted it vertically through a muffler. The total mass flow through the tunnel was controlled by a damper mechanism just prior to the muffler.

E. DATA SENSORS

All data were taken with two calibrated Prandtl-type pitot-static probes, one measuring three-and-a-half inches and the other eighty-three hundredths inch, stem to tip, thus allowing acquisition of data between test section data stations. Two U-tube manometers were connected to the probes so that direct readout of local static and dynamic pressure was obtained. These manometers, shown in Fig. 5, could be inclined at any angle between two and forty-five degrees, providing a wide range of sensitivity. A similar manometer was connected to the nozzle static pressure ports so that the test section inlet dynamic pressure could be continuously monitored.

The traversing mechanism used to position the pitot-static probes in the wake was hand-operated and completely detachable from the tunnel. The probe was clamped firmly in its movable support fixture on the traverse which was moved

vertically by a screw drive mechanism. Probe position could be determined to within a hundredth of an inch with the aid of a ruled indicator on the traverse.

III. EXPERIMENTAL PROCEDURE

A. TEST SECTION PREPARATION

The test section was configured to produce both a favorable-only pressure gradient (Figure 6), and an adverse-favorable pressure gradient (Figure 3) over its entire length. For ease in setting the flexible walls to the desired profile, two reference lines were scribed at the top and bottom of the right hand vertical wall of the test section. All dimensions given in Table I are referenced to these lines and indicate the distance in inches from these reference lines to the flow side of the flexible walls.

The following procedure was used in setting the flexible walls. Proceeding from the test section inlet, the right side of each adjustment fixture was set to the desired position and tightened. After all eight fixtures had been set, each was re-checked to insure that its setting had not been disturbed. Then, with the aid of a bubble level, the left side of each adjustment fixture was moved until the wall was level. Even though the walls could only be set precisely to the desired dimensions at the eight adjustment points, the resulting area distribution in the test section never varied more than five percent from the desired area. The only variance occured when the axial area gradient was large, such as at the beginning of the favorable pressure gradient profile or in the transition section of the adverse-favorable

pressure gradient profile; otherwise the wall profile conformed exactly to the desired area distribution.

B. DATA ACQUISITION

All data were recorded from the water-filled U-tube manometers (Figure 5) connected to the pitot-static tubes and nozzles. A scale was placed between the tubes of each manometer providing a minimum reading of a hundredth of an inch deflection on the slant height. To eliminate any possible parallax and to assure consistent readings from the manometers, a portable plastic sight unit was placed over the manometer scale. This unit restricted one's line of sight to a plane perpendicular to the manometer.

At each position of the probe in the wake, the manometer readings were recorded and plotted on a graph so that it was immediately obvious when more data was needed in a particular portion of the wake. This technique was particularly advantageous in determining the exact center of the wake and the point where the freestream was encountered.

The high turbulence intensity in the central core of the wake caused large fluctuations in the manometer water columns. These fluctuations were often as great as two-tenths inch even at manometer inclinations of thirty degrees. By observing the fluctuations for several minutes at each probe position in the wake, it was possible to "average" these fluctuations by eye and obtain a reading that was accurate to within an estimated five-hundredths of an inch.

The inclination (set with an inclinometer) of each of the three U-tube manometers was varied according to tunnel operating conditions and axial location of the pitot-static probe. For a given axial data station and local flow velocity, an inclination was chosen that would yield approximately a ten to eleven inch difference in water column slant height when the probe was positioned in the freestream. This assured adequate sensitivity and readability of the water columns at the lower velocities of the wake centerline.

Traversing of the wake by the pitot-static probe was always done from the upper free stream edge to the lower free stream edge. The free stream was located by moving the probe away from the upper wall until the maximum slant height difference on the dynamic pressure manometer remained unchanged for a few tenths of an inch below the point at which it first occurred. This point was taken as the free stream. The lower free stream was found in the same way.

IV. DISCUSSION OF RESULTS

A. TEST SECTION

A qualitative indication of the linearity of the test section pressure gradient in both the favorable and the adverse-favorable configurations can be seen in Figures 7, 8. The limitations of the test section in generating an exactly linear pressure distribution result from the lack of completely flexible upper and lower test section wall and from the limited number of wall adjustment points from which to set the area profile. Considering these physical limitations and the fact that the desired area distribution in the test section was derived from one-dimensional analysis, the resulting actual pressure distribution in the test section is quite good. A comprehensive program to calibrate the test section was not undertaken since only a qualitative idea of its performance was necessary for this investigation.

B. EXPERIMENT

The experiment was designed to compare the decay of two similar wakes which have had different flow histories. This was done, within the physical constraints of the test section, by using a two-inch diameter wake generator in a favorable pressure gradient channel sixty eight inches long and a one-inch diameter wake generator in an adverse-favorable pressure gradient channel with the favorable pressure gradient

occupying the downstream thirty four inches (Figures 3 and 8). The two wakes are compared within the favorable pressure gradient regions downstream of the point where both wakes have the same velocity defect. The approximate solution of the integral momentum equation in Appendix C illustrates the possibility that an adverse pressure gradient can sustain a wake deficit, such as the one studied here. In addition, the wakes are compared at the same relative non-dimensional distance into the favorable pressure gradient. This was possible because the favorable pressure gradient lengths were in the same ratio as the initial wake widths. It is apparent from the experimental data in Figure 9 that the velccity defect decays rapidly when the flow enters the favorable pressure gradient directly from the nozzle. However, the velocity defect persists [Figure 10] and then decays at a much slower rate [Figure 11] when the flow has previously encountered an adverse pressure gradient. Since the rate at which the velocity defect diminishes is directly related to the eddy viscosity, it can be at least qualitatively concluded from Figures 12,13 that the eddy viscosity of a turbulent wake is a function of the flow history and its effect on the turbulent field. Classically, it is assumed that the eddy viscosity is purely a function of the local mean flow properties, we must conclude that care must be exercised when applying classical eddy viscosity models to pressure gradient situations. In order to test this

conclusion, a numerical analysis of the experimental data was conducted.

C. COMPUTER PROGRAM

The data analysis computer program uses a forward difference scheme to solve the equations of motion for the turbulent shear coefficients (CTAU) and the eddy viscosities (EDDY) as described in Appendices B and D. The experimental data obtained from the wind tunnel were used to test the program and assure correct processing with no coding errors. The numbers generated for CTAU and EDDY were unreasonably large and therefore the results are inconclusive. It is felt that the increments in the data in the axial direction used in finite differencing the data were too large for an accurate approximation of the partial derivatives which appear in the equations (see Appendix B). A better method would be to smooth the data and use a central difference numerical scheme to approximate the partial derivatives. The data taken in the experimental phase of this investigation were not adaptable to the central difference scheme. Given experimental data with sufficiently small increments in the axial direction, the program will provide the correct values for the parameters listed in Appendix D.

V. CONCLUSIONS

The experiment described in this report was designed to test the validity of classical eddy viscosity models in free turbulent mixing situations with axial pressure gradients. The results indicate that those classical models which are explicitly independent of the local turbulence structure will fail to predict the experimentally observed phenomena which are a strong function of the turbulent field. In these pressure gradient situations, the local turbulent kinetic energy is not a unique function of the local non-turbulent mean flow and the influence of the turbulence on the form of the Reynolds stresses must be an explicit one in any eddy viscosity model.

TABLE I

ACTUAL AND THEORETICAL
TEST SECTION GEOMETRY
FAVORABLE AND ADVERSE-FAVORABLE PRESSURE GRADIENTS

		FAVORABLE GRADIENT (2)			ADVERSE-FAVORABLE GRADIENT (2)		
STATION	DOWNSTREAM DISTANCE, INCHES (1)	THEORETICAL TEST-SECTION ORDINATES INCHES	ACTUAL TEST-SECTION ORDINATES, INCHES (TOP)	(BOTTOM)	THEORETICAL TEST-SECTION ORDINATES INCHES	ACTUAL TEST-SECTION ORDINATES, INCHES (TOP)	(BOTTOM)
1	4.0	2.59	2.08	2.09	8.29	8.30	8.31
2	9.0	4.27	4.30	4.28	7.96	7.97	7.96
3	14.0	5.29	5.47	5.50	7.52	7.65	7.64
4	19.0	5.99	6.01	5.99	6.90	6.87	6.89
5	24.0	6.50	6.50	6.49	5.91	5.43	5.45
6	29.0	6.91	6.91	6.90	4.00	3.99	3.98
7	34.0	7.23	7.26	7.24	--	3.45	3.33
8	39.0	7.50	7.50	7.50	4.00	4.03	4.03
9	44.0	7.73	7.75	7.73	5.89	5.45	5.45
10	49.0	7.93	7.90	7.95	6.87	6.86	6.87
11	54.0	8.10	8.10	8.13	7.49	7.60	7.59
12	59.0	8.25	8.25	8.27	7.93	7.93	7.93
13	64.0	8.39	8.39	8.38	8.26	8.28	8.25

NOTES: (1) REFERENCED TO TEST SECTION INLET

(2) REFERENCED TO SCRIBED LINES 12-INCHES FROM THE TEST SECTION CENTERLINE AT TOP AND BOTTOM OF TEST SECTION AND MEASURED TOWARDS TEST SECTION CENTERLINE TO FLOW SIDE OF ADJUSTABLE WALL

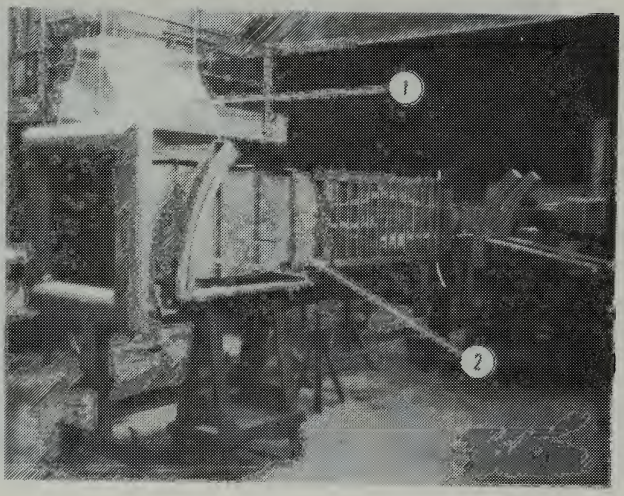

Figure 1

View of tunnel showing nozzles used with (1) favorable pressure gradient and (2) adverse-favorable pressure gradient test section configurations.

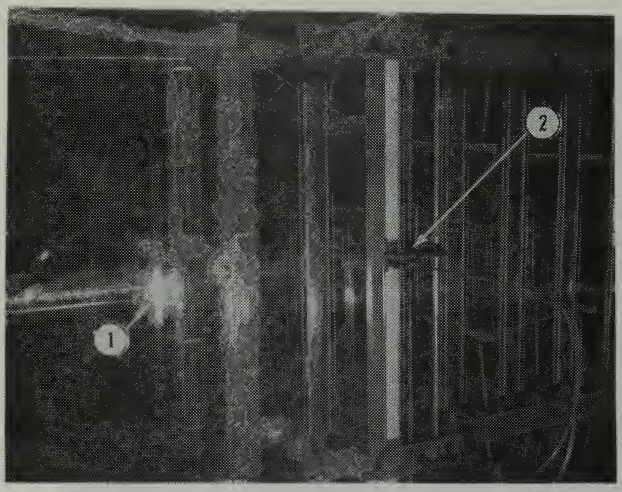

Figure 2

View of Plexiglass nozzle and test section showing (1) 2-inch wake generator installed in the nozzle and (2) the pitot tube traverse mechanism.

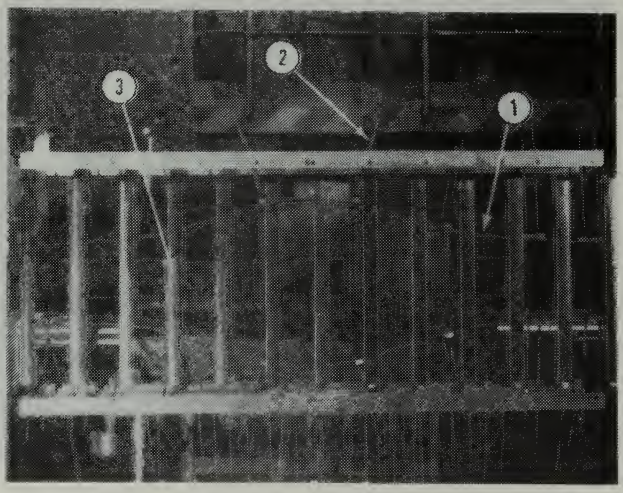

Figure 3

View of Plexiglass test section showing (1) the adjustable walls in the adverse-favorable pressure gradient configuration, (2) the adjusting rods for these walls and (3) the slots through which the pitot tubes are inserted.

Figure 4

Overall view of the wind tunnel showing the diffuser, centrifugal blower and its muffler at extreme right in picture.

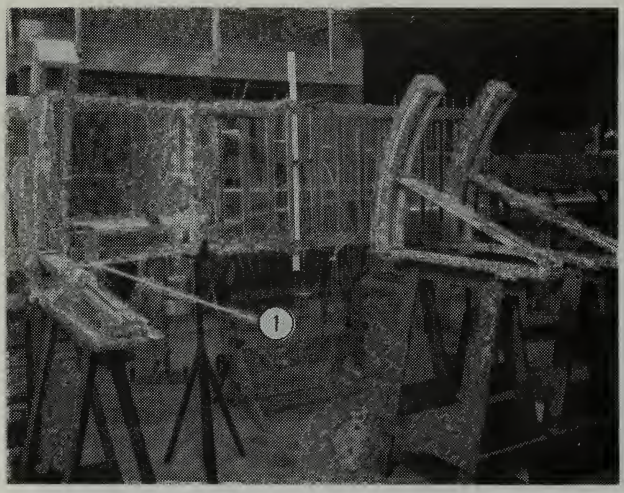

Figure 5

View of inclined U-tube manometers used to obtain pressure readings in the nozzle and test section. The sight unit (1) used to eliminate parallax in reading the manometers is shown on the left.

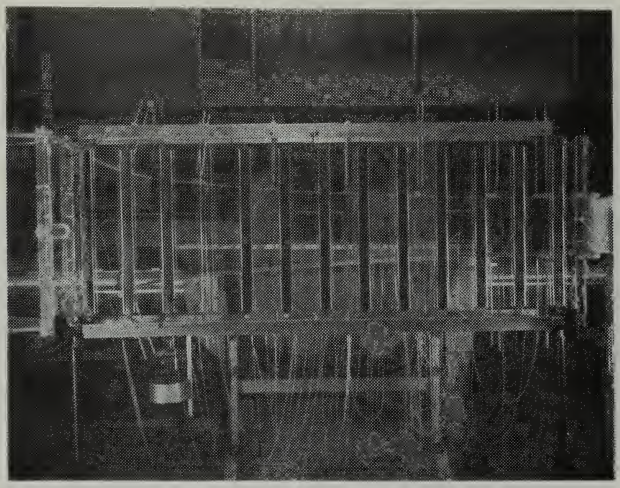

Figure 6

Test section configured for the favorable pressure gradient. The milled slot through which the pitot tube is inserted can be seen at station 4.

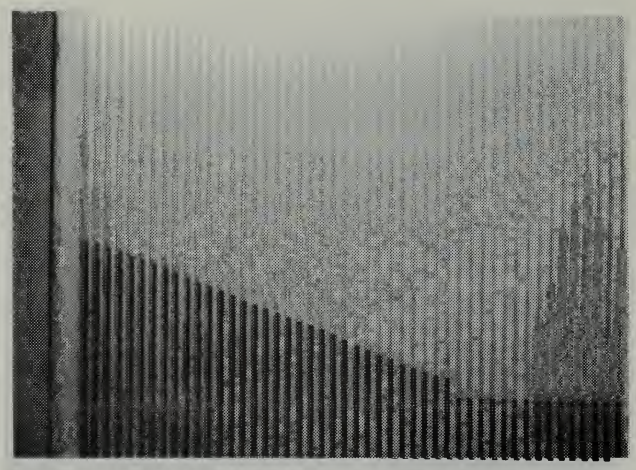

Figure 7

View of manometer bank connected to the static pressure ports along the test section centerline. Shown is the linear pressure distribution in the test section resulting from the configuration in Fig. 6. The horizontal water columns are not connected to the tunnel.

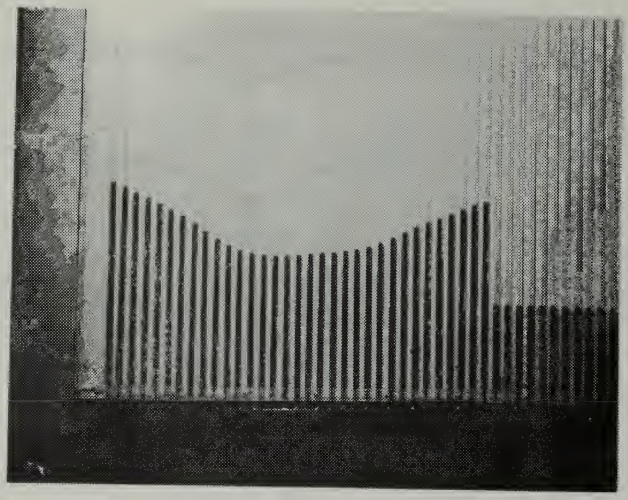

Figure 8

View of manometer bank connected to the static pressure ports along the test section centerline. Shown is the pressure distribution in the test section resulting from the configuration in Fig. 3. The horizontal water columns are not connected to the tunnel.

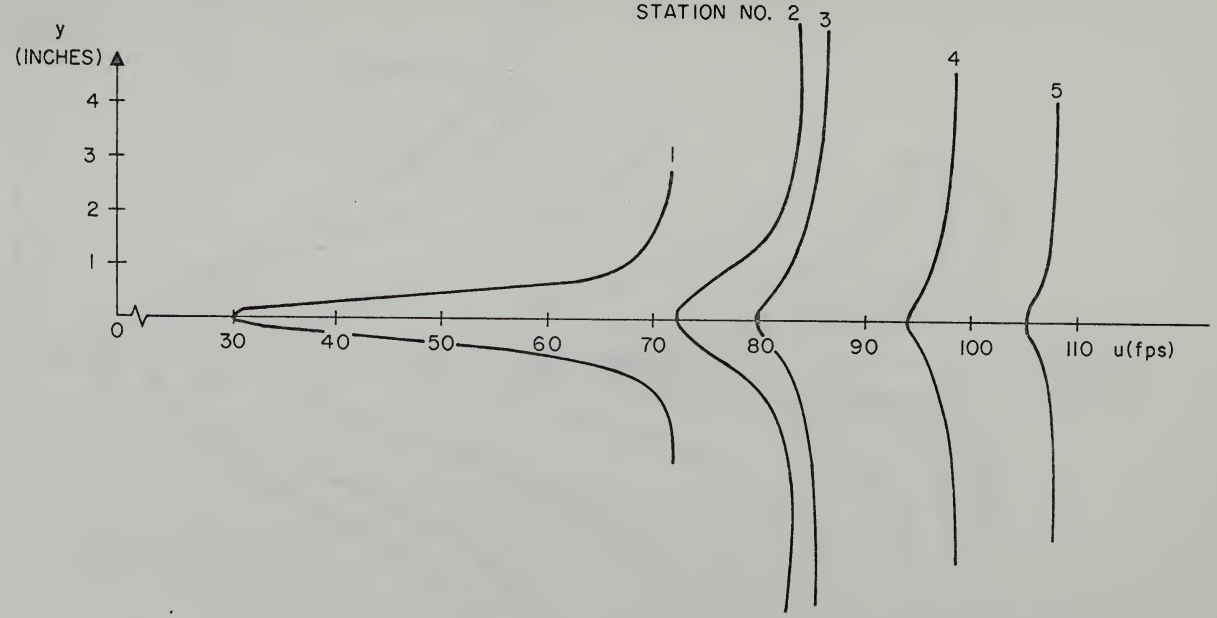

FIG. 9. VELOCITY PROFILES IN A FAVORABLE-ONLY PRESSURE GRADIENT
(2" DIAMETER WAKE GENERATOR, 68 $\frac{1}{2}$" GRADIENT LENGTH)

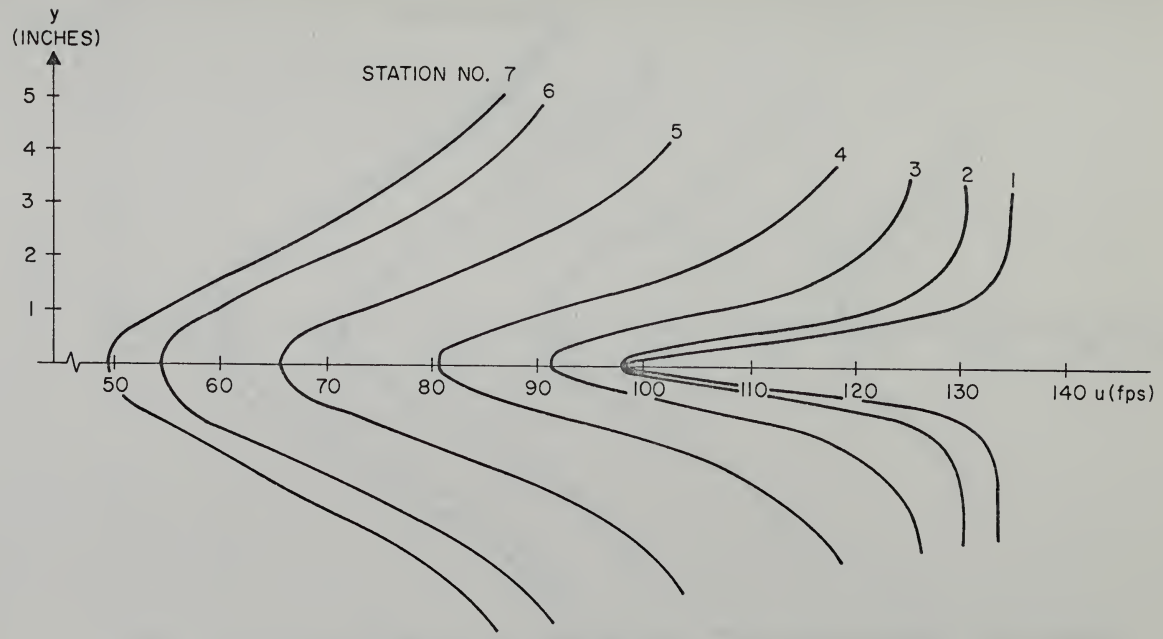

FIG. 10. VELOCITY PROFILES IN ADVERSE PRESSURE GRADIENT (1" DIAMETER WAKE GENERATOR, 29 $\frac{1}{2}$ " GRADIENT LENGTH)

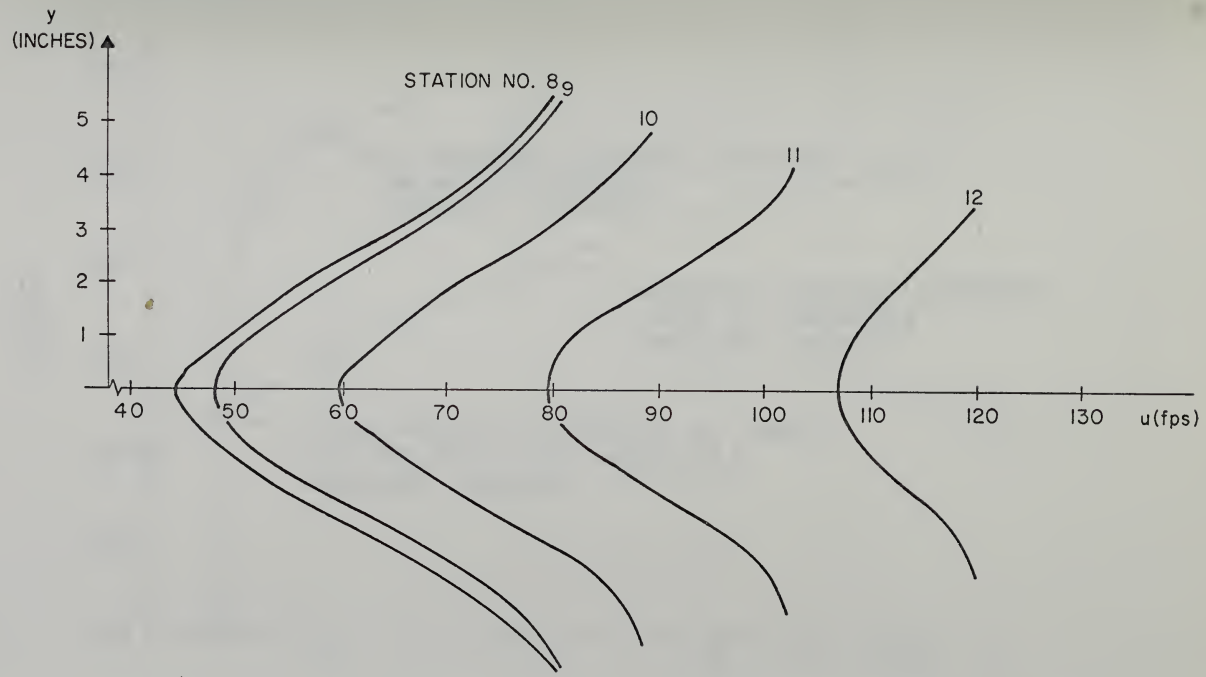

FIG. 11. VELOCITY PROFILES IN A FAVORABLE PRESSURE GRADIENT, FOLLOWING AN ADVERSE PRESSURE GRADIENT
(1" WAKE GENERATOR, $29\frac{1}{2}$" F. P. G. LENGTH)

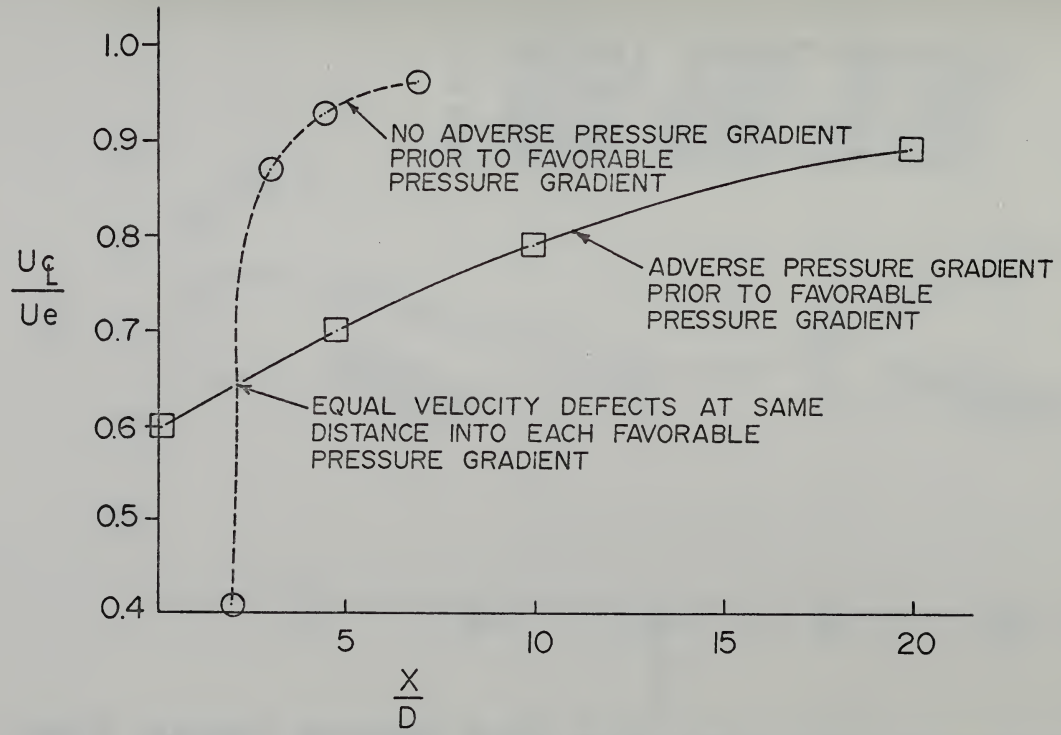

FIG. 13. COMPARISON OF VELOCITY RECOVERY RATES IN THE TWO LINEAR FAVORABLE PRESSURE GRADIENTS

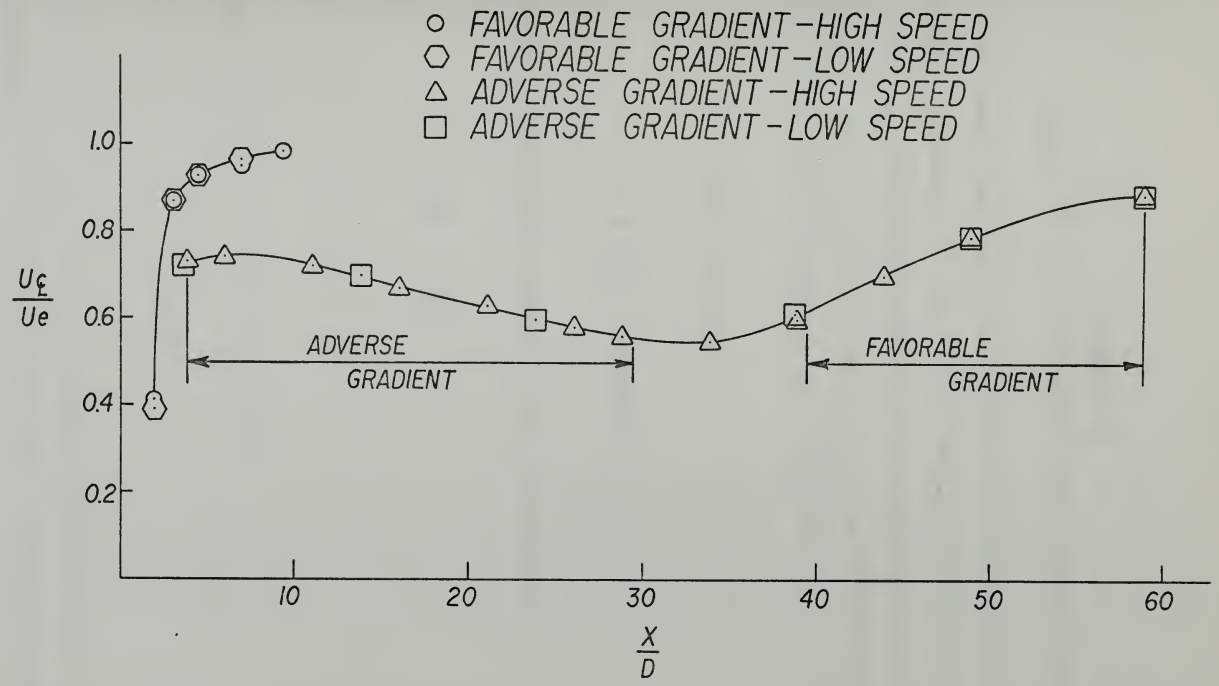

FIG. 12 VELOCITY RECOVERY RATES IN BOTH TEST SECTION CONFIGURATIONS

APPENDIX A

DESIGN OF THE TEST SECTION AREA DISTRIBUTION

The local cross-sectional area of the test section and the static pressure of the fluid flowing through the section are related through the equation of continuity and Bernoulli's equation. For the steady, isentropic flow of an incompressible fluid, these equations can be written:

$$VA = \text{constant} \tag{1}$$

$$p + \frac{1}{2}\rho V^2 = \text{constant} \tag{2}$$

In the log-derivative plane (1) and (2) become

$$\frac{dV}{V} = -\frac{dA}{A} \tag{3}$$

$$dp = -\rho V^2 \frac{dV}{V} \tag{4}$$

Substitution of (3) into (4) yields

$$dp = \rho V^2 \frac{dA}{A} \tag{5}$$

From (1) $V = C_1/A$, where C_1 is the volumetric flow rate at the inlet to the test section. Thus, (5) can be written

$$\frac{dp}{dx} = \rho \frac{C_1^2}{A^3} \frac{dA}{dx} \tag{6}$$

After specifying a particular pressure gradient, (6) can be solved to determine the required area distribution.

For a constant pressure gradient, $\frac{dp}{dx} = -C_2$, and integration of (6) for this simple case is straightforward. The result can be written

$$\frac{A(x)}{A_1} = \frac{1}{1 + \beta x} \tag{7}$$

where $\beta = C_2/q_1$, A_1 is the test section inlet area and q_1 is the dynamic pressure at the test section inlet. For a specified inlet and exit area

$$\beta = \frac{A_1^2 - A_2^2}{A_2^2 L} \tag{8}$$

where L is the length of the pressure gradient, and A_2 is the channel area at x = L.

The area profiles for the favorable and adverse-favorable pressure gradients used during this investigation are shown in Figs. 3 and 6, respectively. Table I contains the specific dimensions used to set the flexible walls of the test section to the desired area profile. Shown for comparison in this table are measurements of the upper and lower flexible walls as they were set prior to taking data. The differences in

dimensions, where they exist, between the theoretical and actual wall settings show the degree of conformity of the flexible walls to the desired profile.

APPENDIX B

DEVELOPMENT OF AN EQUATION FOR CALCULATION OF THE LOCAL TURBULENT SHEAR COEFFICIENT

The momentum equation governing the mean flow properties of a steady, two-dimensional, incompressible turbulent shear flow can be written, using Reynolds' averaging technique [Ref. 3]:

$$\bar{u}\frac{\partial \bar{u}}{\partial x} + \bar{v}\frac{\partial \bar{u}}{\partial y} = -\frac{1}{\rho}\frac{d\bar{p}}{dx} + \frac{1}{\rho}\frac{\partial \tau}{\partial y} \qquad (1)$$

where $\tau \equiv -\rho\overline{u'v'}$ and $\rho\overline{u'^2}$ has been neglected with respect to $\bar{p}$. The same arguments which Prandtl used to derive equation (1) from the Navier-Stokes equations, in the case of a boundary layer, are directly applicable to a two-dimensional wake in approximately parallel flow through a rectangular duct. Introducing the integrated form of the continuity equation

$$\bar{v} = -\int_0^y \left(\frac{\partial \bar{u}}{\partial x}\right) dy \qquad (2)$$

into equation (1) transforms it to

$$\bar{u}\frac{\partial \bar{u}}{\partial x} - \frac{\partial \bar{u}}{\partial y}\int_0^y \left(\frac{\partial \bar{u}}{\partial x}\right) dy = -\frac{1}{\rho}\frac{d\bar{p}}{dx} + \frac{1}{\rho}\frac{\partial \tau}{\partial y} \qquad (3)$$

By non-dimensionalizing equation (3) with respect to the local freestream velocity, u_e, and utilizing the product rule

of differential calculus, equation (3) becomes

$$\frac{\bar{u}}{u_e}\left(\frac{\bar{u}}{u_e}\right)_x + \left(\frac{\bar{u}}{u_e}\right)^2 \frac{u_{e_x}}{u_e} - \left(\frac{\bar{u}}{u_e}\right)_y \int_0^y \left(\frac{\bar{u}}{u_e}\right)_x dy - \left(\frac{\bar{u}}{u_e}\right)_y \left(\frac{u_{e_x}}{u_e}\right) \int_0^y \left(\frac{\bar{u}}{u_e}\right) dy$$

$$= -\frac{1}{\rho u_e^2} \bar{P}_x + \frac{C_\tau y}{2} \qquad (4)$$

where $C_\tau = 2\tau/\rho u_e^2$ and subscripts x and y indicate partial differentiation with respect to x and y. Equation (4) is now integrated from y = 0 to y = y_τ, an arbitrary point in the wake, and relax the condition that equation (4) be satisfied at every point in the flow, allowing it to be satisfied on the average between y = 0 and y = y_τ. After the necessary integration by parts and considerable manipulation, the final equation for the turbulent shear coefficient, C_τ, can be written

$$\frac{C_\tau(y_\tau)}{2} = \int_0^{y_\tau} \left[2\left(\frac{\bar{u}}{u_e}\right) - \frac{\bar{u}(y_\tau)}{u_e}\right]\left[\left(\frac{\bar{u}}{u_e}\right)_x + \left(\frac{\bar{u}}{u_e}\right)\left(\frac{u_{e_x}}{u_e}\right)\right] dy + \int_0^{y_\tau} -\frac{1}{\rho u_e^2} \bar{P}_x \, dy \qquad (5)$$

Equation (5) was solved numerically with the computer program listed in Appendix D.

The validity of equation (5) can be checked by letting

$$y_\tau \to \infty$$

$$u(y_\tau) \to u_e, \qquad \frac{\partial \bar{u}}{\partial y}(y_\tau) \to 0$$

$$\frac{d\bar{P}}{dx} = -\rho u_e \frac{du_e}{dx}$$

Thus $C_\tau(y_\tau) = 0$ and equation (5) reduces to

$$\frac{d\theta}{dx} + \frac{1}{u_e}\frac{du_e}{dx}(2\theta + \delta^*) = 0 \qquad (6)$$

where

$$\theta \equiv \int_0^\infty \frac{\bar{u}}{u_e}\left(1 - \frac{\bar{u}}{u_e}\right) dy$$

$$\delta^* \equiv \int_0^\infty \left(1 - \frac{\bar{u}}{u_e}\right) dy$$

Equation (6) is the well known momentum integral equation in boundary layer theory.

APPENDIX C

SOLUTION TO THE MOMENTUM INTEGRAL EQUATION

The momentum integral equation obtained in Appendix B can be integrated in the special case of a constant pressure gradient. From Eq. (6) in Appendix B

$$\frac{d\theta}{dx} + \frac{1}{u_e} \frac{du_e}{dx} (2\theta + \delta^*) = 0 \qquad (1)$$

where θ, δ^* are the momentum and displacement thickness defined in Appendix B.

An expression for $\frac{du_e}{dx}$ can be obtained from the inviscid Bernoulli equation

$$\frac{du_e}{dx} = - \frac{1}{\rho u_e} \frac{dp}{dx} \qquad (2)$$

Substitution of Eq. (2) into Eq. (1) yields a differential equation in terms of θ, $\frac{dp}{dx}$, and $H \equiv \delta^*/\theta$ (the shape factor).

$$\frac{d}{dx}(\ln \theta) - \frac{1}{\rho u_e^2} \left(\frac{dp}{dx}\right) (H + 2) = 0 \qquad (3)$$

The solution of Eq. (3) is

$$\frac{\theta}{\theta_1} = \exp\left[\int_0^x \frac{1}{\rho u_e^2} \left(\frac{dp}{dx}\right) (H + 2) dx \right] \qquad (4)$$

From Appendix A, $\frac{dp}{dx} = -\beta q_1$ and the integrand of Eq. (4) can be written

$$-\left(\frac{\beta q_1}{2q_e}\right)(H + 2) \tag{5}$$

From the results of Appendix A, the ratio is a known function of x

$$\frac{q_1}{q_e} = \frac{1}{1 + \beta x} \tag{6}$$

After substituting Eqs. (5), (6) into Eq. (4) and integrating, the final solution becomes

$$\frac{\theta}{\theta_1} = \frac{1}{1 + \beta x} \exp\left[\int_0^x \frac{\beta H}{2(1 + \beta x)}\, dx\right] \tag{7}$$

Thus, experimentally derived values for the shape factor can be substituted into Eq. (7), and the resulting value of θ can be compared with the experimentally obtained values.

For the restrictive case, H = constant, we can extend this solution to

$$\frac{\theta}{\theta_1} = \frac{1}{(1 + \beta x)^{1+H/2}} \tag{8}$$

Further, for $H \simeq 1.0$ (a close approximation under the conditions of this investigation), Eq. (7) reduces to

$$\frac{\theta}{\theta_1} \simeq \frac{1}{(1 + \beta x)^{3/2}} \qquad (9)$$

This result compares favorable with experimental data and serves as a guide for calculating the growth or decay of wakes in pressure gradients.

APPENDIX D

DATA REDUCTION PROGRAM

A. GENERAL

The following FORTRAN IV computer program uses the experimental values of dynamic and static pressure through the wake in inches of water and calculates the wake momentum thickness, displacement thickness, turbulent shear coefficient, eddy viscosity, and Prandtl mixing length. The results are printed out as well as plotted on the calcomp plotter.

B. NOMENCLATURE

The following parameters and arrays are used in the program, with their respective dimensions shown in parentheses:

ALV - array used to store interpolated values of dynamic pressures (feet)

AMIXL - local Prandtl mixing length in the wake (feet)

CTAU - local turbulent shear coefficient for each point in the wake

DELRAT - ratio of succeeding DELSTR's to that at the first data station

DELSTR - wake displacement thickness (feet)

DELX - axial distance between succeeding probe tip positions (feet)

DIAMTR - diameter of wake generator (inches)

EDDY - eddy viscosity

EPSIL - residual in momentum integral equation when experimental values for THETA and SHAPE are substituted into it

LABEL - label for subroutine DRAW

MN - number of data points laterally through the wake

MX - number of axial data positions

MY - number of points (always odd) into which the wake is divided

P - array of local static pressures for each point in the wake (psf)

PATM - atmospheric pressure (inches of mercury)

Q - freestream dynamic pressure (psf)

SHAPE - wake shape factor (DELSTR/THETA)

THETA - wake momentum thickness (feet)

THETAP - inclination of static pressure manometer (degrees)

THETAV - inclination of dynamic pressure manometer (degrees)

THRAT - ratio of succeeding THETA's to that at the first data station

TITLE1 - title for subroutine DRAW

TITLE4 - title for subroutine DRAW

U - array of velocities for each point in the wake (feet per second)

URATIO - ratio of local wake velocity to local free-stream velocity

XIN - array of probe traverse positions through the wake (inches)

XOUT - interpolated probe traverse positions for each of the MY points in the wake (inches)

XPOS - probe tip position measured from downstream side of the wake generator (inches)

YOUT - interpolated manometer readings (for YQ and YPS) for each of the MY points through the wake (inches)

YPS - static pressure manometer slant distance height difference (inches)

YQ - dynamic pressure manometer slant distance height difference (inches)

C. SUBROUTINES

INTEG - uses Simpson's rule to numerically integrate the function F. It must be supplied with K points (always odd) equally spaced, DELX units apart.

PIF2 - second-order interpolation function. X is the point for which interpolation is desired. XLIST and FLIST contain the N number of abscissas and ordinates, respectively, of the table to be interpolated.

DECIDE - insures that the wake is divided into an odd number of points spaced 0.1 inches apart. If the wake contains an even number of experimental data points (found by subtracting the lower traverse position from the upper position and multiplying by ten), DECIDE adds a point onto the upper edge of the wake and sets its value equal to the freestream value. The total number of points are printed out.

FILL - insures that the wake at succeeding downstream data positions contains as many data points as the one before it. Thus division by zero is precluded in the computation scheme used for EPSIL and CTAU. If the succeeding data station has fewer points in its wake, FILL copies the uppermost wake point (the freestream point) into additional points as necessary to equal the number of points at the current position.

DRAW - SSP3 subroutine for the IBM 360/67 at the Naval Postgraduate School which uses the CALCOMP plotter to graph the program output.

D. USAGE

The program will accept up to twelve data positions in the streamwise direction. If more than that number are required, the dimensions of the appropriate arrays (ALP, ALV,U,P,A,B,C,D,EDDY,AMIXL,XOUT,URATIO,CTAU,DELSTR,THETA, SHAPE,EPSIL,Q,DELRAT,THRAT,THETAV,THETAP,PATM,XPOS,DELY, NUM) will have to be modified accordingly. The program is set up for exactly three complete runs (a run is defined as the processing of data taken for a particular test section configuration and inlet dynamic pressure). If more or fewer runs are necessary, the limits for the KK DO-LOOP have to be modified accordingly. There is no restriction on the number of data points that can be obtained at each axial data position. Subscript I always refers to each axial position for which data was taken, and subscript J always refers to the points through the wake, at a given axial data position.

The following input data is supplied by the user in the order presented. Input format is given in parentheses.

Two cards: TITLE1 (6A8) - first graph title

Two cards: TITLE4 (6A8) - second graph title

One card: LABEL (12A4) - curve label. One number in each four columns to designate the data position, i.e. 1 2 3 4, etc.

For each run the following data is needed:

One card: run identification (up to 47 characters)

One card: number of data positions (I2); wake generator diameter, DIAMTR inches , (F10.2)

One or more cards: THETAV, degrees (8F10.1)

One or more cards: THETAP, degrees (8F10.1)

One or more cards: PATM, inches (8F10.2)

One or more cards: XPOS, inches (8F10.2)

One card: data position identification (up to 47 characters)

One or more cards: XIN, inches (8F10.3)

One or more cards: YQ, inches (8F10.3)

One or more cares: YPS, inches (8F10.3)

E. PROGRAM LISTING

A listing of the program which has been described here is included on the following six pages.

```
      IMPLICIT REAL*4 (A-H,O-Z)
      REAL*8  TITLE1(12)
      REAL*8  TITLE4(12)
      REAL*8  LABEL1/'    DELS'/
      REAL*8  LABEL2/'    THET'/
      REAL*8  LABEL3/'    SHAP'/
      REAL*4  LABEL(12)
      DIMENSION ALP(12,125),ALV(12,125),U(12,125),P(12,125)
      DIMENSION A(12,125),B(12,125),C(12,125),D(12,125)
      DIMENSION EDDY(12,125),AMIXL(12,125),XOUT(12,125)
      DIMENSION URATIO(12,125),CTAU(12,125),YQ(30),YPS(30)
      DIMENSION UR(125),UP(125),UC(125),UD(125),F(125)
      DIMENSION YOUT(125),XIN(30)
      DIMENSION AXIS(125)
      DIMENSION DELSTR(12),THETA(12),SHAPE(12),EPSIL(12)
      DIMENSION Q(12),DELRAT(12),THRAT(12),THETAV(12)
      DIMENSION THETAP(12),PATM(12),XPOS(12),DELY(12)
      DIMENSION NUM(12)
      COMMON/A/ H
      EQUIVALENCE (F(1),YOUT(1),UR(1),UP(1),UC(1),UD(1))
      EQUIVALENCE  (A(1,1),EDDY(1,1))
      EQUIVALENCE  (B(1,1),AMIXL(1,1))
      EQUIVALENCE (C(1,1),AXIS(1))
      DATA GAMA/62.32/,RHO/0.002378/
      H=0.1E0
      Y=H/12.0
C
C
  50  FORMAT('
     1')
  51  FORMAT(I2,F10.2)
  52  FORMAT(8F10.1)
  53  FORMAT(8F10.2)
  54  FORMAT('
     1')
  55  FORMAT(I2)
  56  FORMAT(8F10.3)
  57  FORMAT(///////' ',T20,6A8)
  58  FORMAT(///////' ',T20,12A4)
  70  FORMAT(//////////' ',T33,'ECHO-CHECK DATA'///)
  71  FORMAT(//' ',T20,'THETAV',(' ',T33,8F10.2//))
  72  FORMAT(//' ',T20,'THETAP',(' ',T33,8F10.2//))
  73  FORMAT(//' ',T20,'PATM',(' ',T33,8F10.2//))
  74  FORMAT(//' ',T20,'XPOS',(' ',T33,8F10.2//))
  75  FORMAT(///' ',T53,'MN=',I3///)
  76  FORMAT(//' ',T10,'XIN',(' ',T21,8F10.3//))
  77  FORMAT(//' ',T10,'YQ ',(' ',T21,8F10.3//))
  78  FORMAT(//' ',T10,'YPS',(' ',T21,8F10.3//))
  79  FORMAT('1',T50,'***RESULTS OF DATA REDUCTION***')
  80  FORMAT(//////' ',T50,'AXIAL STATION',I2,'OUT OF',I2,
     1'STATIONS'/////)
  81  FORMAT(' ',T18,'DELSTAR=',G12.5,5X,'THETA=',G12.5,5X,
     1'SHAPE=',G12.5,5X,'EPSILON=',G12.5)
  82  FORMAT(//////' ',T8,'POINT',T30,'U',T48,'U/UE',T70,'P'
     1,T88,'CTAU')
  83  FORMAT('0',T9,I3,T24,G12.5,T44,G12.5,T64,G12.5,T84,
     1G12.5)
  84  FORMAT('1',T44,'***SUMMARY OF INTEGRATED WAKE PROPER',
     1'TIES***')
  85  FORMAT(/////' ',T3,'AXIAL',T75,'THETA'/' ',T2,'STATION
     1',T16,'X/D',T29,'DELSTAR',T44,'DELRATIO',T60,'THETA',
     2T75,'RATIO',T90,'SHAPE',T105,'EPSILON')
  86  FORMAT('0',T4,I3,T11,G12.5,T26,G12.5,T41,G12.5,T56,
     1G12.5,T71,G12.5,T86,G12.5,T102,G12.5)
  87  FORMAT('1',T49,'***REYNOLD"S MIXING LENGTH DATA***')
  88  FORMAT(//////' ',T61,'STATION',I3///' ',T44,'POINT',
     1T59,'EDDY VISCOSITY',T79,'MIXING LENGTH')
  89  FORMAT(' ',T45,I3,T60,G12.5,T80,G12.5)
  90  FORMAT(6A8)
  91  FORMAT(//' ','LAST=',I3)
  92  FORMAT(12A4)
```

```
      READ(5,90)  TITLE1
      READ(5,90)  TITLE4
      READ(5,92)  LABEL
C
C     ZERO ALL ARRAYS BEFORE COMPUTATION BEGINS
      F(J)=Z
C
      DO 1000 KK=1,3
      Z=0.0
      DO 1 J=1,125
      DO 1 I=1,12
      XOUT(I,J)=Z
      ALP(I,J)=Z
      ALV(I,J)=Z
      U(I,J)=Z
      URATIO(I,J)=Z
      P(I,J)=Z
      A(I,J)=Z
      B(I,J)=Z
      C(I,J)=Z
      D(I,J)=Z
      CTAU(I,J)=Z
      DELSTR(I)=Z
      THETA(I)=Z
      SHAPE(I)=Z
      EPSIL(I)=Z
      Q(I)=Z
      DELRAT(I)=Z
      THRAT(I)=Z
      THETAV(I)=Z
      THETAP(I)=Z
      PATM(I)=Z
      XPOS(I)=Z
      DELY(I)=Z
1     CONTINUE
      DO 2 I=1,30
      XIN(I)=Z
      YQ(I)=Z
      YPS(I)=Z
2     CONTINUE
      READ(5,50)
      READ(5,51)  MX,DIAMTR
      READ(5,52)  (THETAV(I),I=1,MX)
      READ(5,52)  (THETAP(I),I=1,MX)
      READ(5,53)  (PATM(I),I=1,MX)
      READ(5,53)  (XPOS(I),I=1,MX)
      WRITE(6,50)
      WRITE(6,70)
      WRITE(6,71)  (THETAV(I),I=1,MX)
      WRITE(6,72)  (THETAP(I),I=1,MX)
      WRITE(6,73)  (PATM(I),I=1,MX)
      WRITE(6,74)  (XPOS(I),I=1,MX)
      WRITE(6,57)  (TITLE1(I),I=1,6)
      WRITE(6,57)  (TITLE4(I),I=1,6)
      WRITE(6,58)  (LABEL(I),I=1,12)
C
C     BEGIN COMPUTATION FOR EACH STATION
C
      MX1=MX-1
      DO 6 I=1,MX
      THETAV(I)=THETAV(I)/57.296
      THETAP(I)=THETAP(I)/57.296
      PATM(I)=PATM(I)*70.73
      XPOS(I)=XPOS(I)/12.0
C
C     READ IN MANOMETER HEIGHTS
C
      READ(5,54)
      READ(5,55)  MN
      READ(5,56)  (XIN(J),J=1,MN)
      READ(5,56)  (YQ(J),J=1,MN)
      READ(5,56)  (YPS(J),J=1,MN)
```

```
C       ECHO-CHECK INPUT
C
        WRITE(6,54)
        WRITE(6,75)  MN
        WRITE(6,76)  (XIN(J),J=1,MN)
        WRITE(6,77)  (YQ(J),J=1,MN)
        WRITE(6,78)  (YPS(J),J=1,MN)
        CALL DECIDE(XIN,MN,MY)
        NUM(I)=MY
C
C       INTERPOLATE FOR MISSING DATA POINTS INSIDE WAKE
C
        XOUT(I,1)=XIN(1)
        DO 21 J=2,MY
        XOUT(I,J)=XOUT(I,1)+FLOAT(J-1)*H
 21     CONTINUE
        DO 3 J=1,MY
        X=XOUT(I,J)
        YOUT(J)=PIF2(X,XIN,MN,YQ)
        ALV(I,J)=YOUT(J)/12.0
        U(I,J)=SQRT(2.0*GAMA*SIN(THETAV(I))*ALV(I,J)/RHO)
 3      CONTINUE
        Q(I)=0.5*RHO*U(I,MY)**2
C
C       CALCULATE DISPLACEMENT THICKNESS
C
        DO 31 J=1,MY
        URATIO(I,J)=U(I,J)/U(I,MY)
        F(J)=1.0-URATIO(I,J)
 31     CONTINUE
        CALL INTEG(F,MY,Y,RESULT)
        DELSTR(I)=RESULT
        DELRAT(I)=DELSTR(I)/DELSTR(1)
C
C       CALCULATE MOMENTUM THICKNESS
C
        DO 4 J=1,MY
        F(J)=URATIO(I,J)*(1.0-URATIO(I,J))
 4      CONTINUE
        CALL INTEG(F,MY,Y,RESULT)
        THETA(I)=RESULT
        THRAT(I)=THETA(I)/THETA(1)
C
C       CALCULATE SHAPE FACTOR IN MOMENTUM INTEGRAL
C
        SHAPE(I)=DELSTR(I)/THETA(I)
C
C       INTERPOLATE P-STATIC MANOMETER READINGS
C
        DO 5 J=1,MY
        X=XOUT(I,J)
        YOUT(J)=PIF2(X,XIN,MN,YPS)
        ALP(I,J)=YOUT(J)/12.0
        P(I,J)=PATM(I)- GAMA*SIN(THETAP(I))*ALP(I,J)
 5      CONTINUE
 6      CONTINUE
C
C       CALCULATE RESIDUAL IN MOMENTUM INTEGRAL EQUATION
C
        DO 7 I=1,MX1
        DELX=XPOS(I+1)-XPOS(I)
        MY=NUM(I)
        IF(NUM(I).GT.NUM(I+1))  CALL FILL(NUM,I,U)
        E1=(THETA(I+1)-THETA(I))/DELX
        E2=THETA(I+1)*(SHAPE(I+1)+2.0)
        E3=(U(I+1,MY)-U(I,MY))/(DELX*U(I+1,MY))
        EPSIL(I+1)=E1+E2*E3
 7      CONTINUE
        EPSIL(1)=0.0
```

```
C      CALCULATE LOCAL TURBULENT SHEAR COEFFICIENT IN WAKE
C
       DO 10 I=1,MX1
       DELX=XPOS(I+1)-XPOS(I)
       MY=NUM(I+1)
       IF(NUM(I).GT.NUM(I+1))  CALL FILL(NUM,I,ALV)
       DO 10 K=1,MY
       DO 9 J=1,K
       A(I+1,J)=2.0*URATIO(I+1,J)-URATIO(I+1,K)
       B(I+1,J)=(URATIO(I+1,J)-URATIO(I,J))/DELX
       C1=URATIO(I+1,J)/U(I+1,MY)
       C2=(U(I+1,MY)-U(I,MY))/DELX
       C(I+1,J)=C1*C2
       D1=SIN(THETAP(I+1))/SIN(THETAV(I+1))
       D2=(ALP(I,J)-ALP(I+1,J))/(DELX*ALV(I+1,MY))
       D(I+1,J)=D1*D2
       F(J)=A(I+1,J)*(B(I+1,J)+C(I+1,J))+D(I+1,J)/2.0
     9 CONTINUE
       CALL INTEG(F,K,Y,RESULT)
       CTAU(I+1,K)=2.0*RESULT
    10 CONTINUE
       WRITE(6,79)
       DO 14 I=1,MX
       WRITE(6,80)  I,MX
       WRITE(6,81) DELSTR(I),THETA(I),SHAPE(I),EPSIL(I)
       WRITE(6,82)
       MY=NUM(I)
       DO 13 J=1,MY
       WRITE(6,83) J,U(I,J),URATIO(I,J),P(I,J),CTAU(I,J)
  13   CONTINUE
  14   CONTINUE
       WRITE(6,84)
       WRITE(6,85)
       DO 15 I=1,MX
       XD=12.0*XPOS(I)/DIAMTR
       WRITE(6,86) I,XD,DELSTR(I),DELRAT(I),THETA(I),THRAT(I)
      1,SHAPE(I),EPSIL(I)
  15   CONTINUE
C
C      CALCULATE EDDY VISCOSITY AND REYNOLD'S MIXING LENGTH
C
       WRITE(6,87)
       DO 17 I=2,MX
       WRITE(6,88) I
       MIN=((NUM(I)-1)/2)+10
       MAX=NUM(I)-10
       DO 16 J=MIN,MAX
       E1=ABS(CTAU(I,J)*Q(I))
       E2=ABS(U(I,J+1)-U(I,J-1))
       E3=2.0*H
       EDDY(I,J)=(E1/RHO)/(E2/E3)
       AMIXL(I,J)=SQRT(E1/(RHO*(E2/E3)**2))
       WRITE(6,89)  J,EDDY(I,J),AMIXL(I,J)
  16   CONTINUE
  17   CONTINUE
C
C      PLOT PACKAGE BEGINS--MAIN PROGRAM ENDS.
C
       AA=0.
       BB=0.
       IF (KK.EQ.3) AA=2.0E00
       IF (KK.EQ.2)  BB=1.0E01
       DO 100 I=1,MX
 100   XPOS(I)=12.*XPOS(I)/DIAMTR
       CALL DRAW(MX,XPOS,SHAPE,1,5,LABEL3,TITLE1,0.,AA,0,0,0,
      10,9,6,0,LAST)
       CALL DRAW(MX,XPOS,THRAT,2,4,LABEL2,TITLE2,0,0,0,0,0,
      10,9,6,0,LAST)
       CALL DRAW(MX,XPOS,DELRAT,3,3,LABEL1,TITLE1,0,0,0,0,0,
      10,9,6,0,LAST)
```

```
      WRITE(6,91)  LAST
      DO 102 I=1,MX
      MY=NUM(I)
      IF(I.EQ.1) K=1
      IF(I.GT.1.AND.I.LT.MX) K=2
      IF(I.EQ.MX) K=3
      DO 101 J=1,MY
      UR(J)=U(I,J)
      AXIS(J)=XOUT(I,J)/DIAMTR
  101 CONTINUE
      LABEL4=LABEL(I)
      CALL DRAW(MY,AXIS,UR,K,0,LABEL4,TITLE4,0.,BB,0,0,0,0,
     19,15,0,LAST)
  102 CONTINUE
      WRITE(6,91)  LAST
 1000 CONTINUE
      STOP
      END


      SUBROUTINE INTEG(F,K,DELX,RESULT)
      IMPLICIT REAL*4 (A-H,O-Z)
      DIMENSION F(1)
C     INTEGRATION BY SIMPSONS RULE
      K1=K-1
      A=F(1)+F(K)
      B=0.0
      DO 1 I=2,K1,2
      SUM=4.0*F(I)
      B=B+SUM
    1 CONTINUE
      C=0.0
      DO 2 I=3,K,2
      SUM=2.0*F(I)
      C=C+SUM
    2 CONTINUE
      RESULT=DELX*(A+B+C)/3.0
      RETURN
      END


      FUNCTION PIF2(X,XLIST,N,FLIST)
      DIMENSION XLIST(1),FLIST(1)
      BLIF(P,Q,R,S,T)=((Q-P)*(S-T)/(R-Q)+S)
      IF(X-XLIST(N)) 2,2,1
  1   I=N-1
      GOTO 5
  2   IF(X-XLIST(1)) 4,4,6
  4   I=1
  5   K=1
      GOTO 30
  6   K=2
  7   DO 8 I=1,N
      IF(X-XLIST(I)) 9,9,8
  8   CONTINUE
      I=N
  9   I=I-1
 30   BLIF1=BLIF(X,XLIST(I),XLIST(I+1),FLIST(I),FLIST(I+1))
 10   IF(K-1) 11,11,12
 11   PIF2=BLIF1
      RETURN
 12   IF((I+2-N)) 13,13,16
 13   IF((I-1)-1) 15,14,14
 14   IF(ABS(XLIST(I-1)-X) - ABS(XLIST(I+2)-X)) 16,15,15
 15   L=I+2
      GOTO 17
 16   L=I-1
 17   BLIF2=BLIF(X,XLIST(I),XLIST(L),FLIST(I),FLIST(L))
      PIF2=BLIF(X,XLIST(I+1),XLIST(L),BLIF1,BLIF2)
 18   RETURN
      END
```

```
      SUBROUTINE DECIDE(X,M,N)
      COMMON/A/ H
      DIMENSION X(1)
 10   FORMAT(///' ',T10,'NUMBER OF POINTS IN WAKE=',I4)
      A=1.0/H
      N=IFIX((X(M)-X(1))*A)
      L=1
      DO 5 K=1,N
      GOTO (1,2), L
 1    L=2
 5    CONTINUE
C     N IS AN ODD NUMBER---OK
      WRITE(6,10)  N
      RETURN
 2    L=1
      IF(K-N) 5,3,3
 3    N=N+1
C     N WAS EVEN AND WE FORCE IT TO BE ODD
      X(M)=X(M)+H
C     THE EXPERIMENTAL DATA SHOULD BE NEARLY THE SAME FOR
C     THIS POINT AS FOR THE ORIGINAL.
      WRITE(6,10)  N
      RETURN
      END


      SUBROUTINE FILL(NUM,I,U)
      IMPLICIT REAL*4 (A-H,O-Z)
      DIMENSION NUM(1),U(12,1)
      M=NUM(I)
      N=NUM(I+1)
      DO 1 J=N,M
      U(I+1,J)=U(I+1,N)
 1    CONTINUE
      WRITE(6,2)  M,N
      WRITE(6,3)  (J(I+1,J),J=N,M)
 2    FORMAT('J',T20,'M=',I3,10X,'N=',I3//)
 3    FORMAT('0',12G10.4/)
      RETURN
      END
```

LIST OF REFERENCES

1. Bird, R.B., Stewart, W.E., and Lightfoot, E.N., Transport Phenomena, pp. 153-174, Wiley, 1965

2. Lin, C.C., Statistical Theories of Turbulence, Princeton Aeronautical Paperbacks, Princeton University Press, 1961.

3. Schlichting, H., Boundary Layer Theory, McGraw-Hill, 1960.

4. Schubauer, G.B., and TCHEN, C.M., Turbulent Flow, Princeton Aeronautical Paperbacks, Princeton University Press, 1959.

INITIAL DISTRIBUTION LIST

		No. Copies
1.	Defense Documentation Center Cameron Station Alexandria, Virginia 22314	2
2.	Library, Code 0212 Naval Postgraduate School Monterey, California 93940	2
3.	Asst Professor G.J. Hokenson (Code 57Hw) Department of Aeronautics Naval Postgraduate School Monterey, California 93940	1
4.	LT Terrance E. Anderson 2306 North Fairlane Fairway Estates Oak Harbor, Washington 98277	1
5.	Chairman Department of Aeronautics Naval Postgraduate School Monterey, California 93940	1

Security Classification

DOCUMENT CONTROL DATA - R & D

(Security classification of title, body of abstract and indexing annotation must be entered when the overall report is classified)

ORIGINATING ACTIVITY (Corporate author)
Naval Postgraduate School
Monterey, California 93940

2a. REPORT SECURITY CLASSIFICATION
Unclassified

2b. GROUP

REPORT TITLE
A Study of Turbulent Wakes in Constant Streamwise Pressure Gradients

DESCRIPTIVE NOTES (Type of report and, inclusive dates)
Master's Thesis; March 1973

AUTHOR(S) (First name, middle initial, last name)
Terrance Edwards Anderson

REPORT DATE	7a. TOTAL NO. OF PAGES	7b. NO. OF REFS
March 1973	65	4

8a. CONTRACT OR GRANT NO.	9a. ORIGINATOR'S REPORT NUMBER(S)
b. PROJECT NO.	
c.	9b. OTHER REPORT NO(S) (Any other numbers that may be assigned this report)
d.	

10. DISTRIBUTION STATEMENT
Approved for public release; distribution unlimited.

11. SUPPLEMENTARY NOTES	12. SPONSORING MILITARY ACTIVITY
	Naval Postgraduate School Monterey, California 93940

13. ABSTRACT

Two-dimensional turbulent wakes in constant adverse and favorable pressure gradients were studied experimentally. The static and dynamic pressures through the wake were obtained with calibrated Pradtl-type pitot-static probes, and a computer program was written to extract from these data the velocity profiles, displacement thickness, momentum thickness, and the shape factor. This program further provides the turbulent shear coefficient, eddy viscosity, and Prandtl mixing length within the wake.

A wind tunnel was designed specifically for this experiment and its construction details are included. The tunnel test section is unique in that it can be adjusted to generate any specified adverse or favorable pressure gradient.

The results of the experiment indicated that the eddy viscosity was a function of the history of the flow rather than of the local mean flow field, as is classically assumed. The reaction of the turbulent wake to a favorable pressure gradient after encountering an adverse pressure gradient was significantly different from the reaction of the wake to only a favorable pressure gradient.

DD FORM 1 NOV 68 1473 (PAGE 1)
S/N 0101-807-6811

Security Classification

A-31408

14. KEY WORDS	LINK A		LINK B		LINK C	
	ROLE	WT	ROLE	WT	ROLE	WT
Turbulent Wakes						
Streamwise Pressure Gradients						

Thesis
A4859 Anderson
c.1
141997
A study of turbulent wakes in constant streamwise pressure gradients.